Exciton polaritons in two-dimensional dichalcogenide layers placed in a planar microcavity: Tunable interaction between two Bose-Einstein condensates

Mikhail I. Vasilevskiy
Centro de Física, Universidade do Minho, Campus de Gualtar, Braga 4710-057, Portugal
and Department of Physics and Materials Science, City University of Hong Kong, Hong Kong

Darío G. Santiago-Pérez
Universidad de Sancti Spiritus "José Martí Pérez", Ave. de los Mártires 360, CP 62100, Sancti Spiritus, Cuba
and CLAF - Centro Latino-Americano de Física, Avenida Venceslau Braz, 71, Fundos, 22290-140, Rio de Janeiro, RJ, Brazil

Carlos Trallero-Giner
Facultad de Física, Universidad de La Habana, Vedado 10400, La Habana, Cuba

Nuno M. R. Peres
Centro de Física, Universidade do Minho, Campus de Gualtar, Braga 4710-057, Portugal

Alexey Kavokin
Physics and Astronomy School, University of Southampton, Highfield, Southampton, SO17 1BJ, United Kingdom;
Spin Optics Laboratory, State University of St-Petersburg, 1, Ulianovskaya, St-Petersburg, 198504, Russia;
and CNR-SPIN, Viale del Politecnico 1, I-00133 Rome, Italy

(Received 30 September 2015; revised manuscript received 28 October 2015; published 22 December 2015)

Exciton-polariton modes arising from interaction between bound excitons in monolayer thin semiconductor sheets and photons in a Fabry-Perot microcavity are considered theoretically. We calculate the dispersion curves, mode lifetimes, Rabi splitting, and Hopfield coefficients of these structures for two nearly 2D semiconductor materials, MoS_2 and WS_2, and suggest that they are interesting for studying the rich physics associated with the Bose-Einstein condensation of exciton polaritons. The large exciton binding energy and dipole allowed exciton transitions, in addition to the relatively easily controllable distance between the semiconductor sheets, are the advantages of this system in comparison with traditional GaAs or CdTe based semiconductor microcavities. In particular, in order to mimic the rich physical properties of the quantum degenerate mixture of two bosonic species of dilute atomic gases with tunable interspecies interaction, we put forward a structure containing two semiconductor sheets separated by some atomic-scale distance (l) using a nearly 2D dielectric (e.g., h-BN), which offers the possibility of tuning the interaction between two exciton-polariton Bose-Enstein condensates. We show that the dynamics of this structure are ruled by two coupled Gross-Pitaevskii equations with the coupling parameter $\sim l^{-1}$.

DOI: 10.1103/PhysRevB.92.245435 PACS number(s): 71.36.+c, 42.65.−k, 75.75.−c

I. INTRODUCTION

Placing a semiconductor structure into a microcavity yields a number of interesting and potentially useful effects related to resonant coupling between the confined light and elementary excitations in the semiconductors, such as excitons [1]. Since the pioneering work of Purcell [2] it was realized that the emission properties of a light-emitting structure in a cavity are changed because of the back action of the reflected light on the emitter. In the strong coupling regime between microcavity (MC) photons modes and semiconductor excitons, collective excitations named exciton polaritons are formed [1]. Studies of these excitations in structures consisting of a quantum well placed in a semiconductor microcavity (two superlattices acting as Bragg mirrors) have been an area of active research in recent years [1,3–5]. Among the most interesting achievements are the polariton laser [6,7] and Bose-Einstein condensation of exciton polaritons [8,9] with collective dynamics of the condensed phase consistent with superfluidity [10]. Experiments in this field are quite demanding in terms of quality of the samples, typically based on GaAs or CdTe multilayer epitaxial structures, which must be grown with very high precision in order to achieve the desired light-exciton coupling.

Recently developed atomically thin layers of semiconducting transition metal dichalcogenides with chemical formula MX_2 (M = Mo, W and X = S, Se) present strong light-matter interactions owing to their direct band gaps and dipole-allowed interband transitions, which can yield relatively high light absorption and intense photoluminescence despite their ultimately small thickness [11,12]. In these materials conduction and valence bands are both dominantly d type, and the band extrema are located at the K and K' points of the Brillouin zone (BZ) [13]. The simplest effective Hamiltonian contains one hopping parameter t, a band gap parameter Δ, and a spin-orbit (SO) interaction energy λ [14]. Without SO splitting the spectrum is symmetric with respect to the midpoint between the top of the valence band (VB) and the bottom of the conduction band (CB),

$$E_{c,v}(\mathbf{q}) = -\frac{\Delta}{2} \pm \sqrt{\frac{\Delta^2}{4} + a^2 t^2 q^2}, \qquad (1)$$

where a is the lattice constant and $\mathbf{q}$ is the in-plane wave vector with respect to the K (K') point of the BZ. For small q the spectrum (1) is parabolic, and one can introduce an effective mass

$$m_{c,v} = \frac{\hbar^2 \Delta}{2a^2 t^2}. \tag{2}$$

The spin-orbit (SO) interaction splits the valence band into two with different spin orientations permutating between the K and K' valleys; the splitting is equal to 2λ. The effective masses of the three bands (one spin-degenerate CB and two VB's) become unequal, although the difference is not too large [15].

The symmetry group of the wave vector at the K and K' points is C_{3h}. Although both conduction and valence band states at these points are composed of d orbitals of the transition metal, those near the bottom of the conduction band have zero angular momentum projection onto the z axis perpendicular to the layer ($M = 0$), while the valence band states near its top correspond to $M = \pm 1$ and, consequently, optical transitions in the vicinity of either the K or K' point are dipole allowed [13,14,16]. For the effective Hamiltonian of Ref. [14] the transition matrix element is [16]

$$\mathbf{P}_{cv}(\mathbf{q} \approx 0) = m_0 v(\tau \mathbf{e}_x + i\mathbf{e}_y), \tag{3}$$

where $\tau = \pm 1$ for the K and K' points, m_0 is free electron mass, $\mathbf{e}_x$ and $\mathbf{e}_y$ are unit vectors, and the "velocity" v is defined (in analogy with graphene) through the hopping parameter and the lattice constant as $v = at/\hbar$ (note that $2m_c v^2 = \Delta$). The value of this velocity can be estimated from the DFT results, for instance, for MoS_2 $v \approx (5-6) \times 10^7$ cm/s. Therefore we can estimate $|\mathbf{P}_{cv}(0)|^2/(2m_0) = m_0 v^2 = \Delta(m_0/2m_c) \approx$ 1.5–2 eV. Even though this value may look rather small (for comparison, this parameter is about 20 eV for the II-VI *bulk* semiconductors), as we shall see below, the oscillator strength is comparable to usual semiconductor MC materials because of the very small exciton Bohr radius characteristic of the MX_2 materials.

Excitonic states in the MX_2 2D semiconductors (2DSCs) have been studied both theoretically and experimentally [12,13,16–20]. In both absorption and photoluminescence spectra, two strong exciton resonances are observed, commonly labeled A and B. They are associated with electronic transitions involving an electron and a hole (from the upper VB for A states and from the lower one for B states), with parallel spins. Since the hole possesses an angular momentum (perpendicular to the plane)$M = \pm 1$, the excitons couple directly to circular polarized light [19], however, because of the alternation of the left-hand and right-hand polarizations between the K and K' points the light can have any polarization within the plane. The lowest energy A and B excitons are analogous to the $1s$ states of a two-dimensional hydrogen model [13], even though the higher energy states do not follow the 2D Rydberg series [18]. The exciton binding energy is quite large in these materials, of the order of hundreds of meV [12,13,16–20], which makes them interesting for studying exciton physics; in particular, many effects can be studied at higher temperatures. Indeed, the observation of strong coupling between excitons and photons using a MoS_2 monolayer embedded in a dielectric microcavity with the formation of exciton-polariton states at room temperature was recently reported [21]. Another potential advantage is that 2DSCs are rather tolerant in terms of assembling into heterostructures. Because of the van der Waals-type bonding between layers, restrictions related to lattice matching are relaxed [11,22] compared to traditional semiconductors where molecular beam epitaxy is required to produce high quality heterostructures. Also, one can mimic multiple quantum well structures by combining MX_2 layers with a monolayer thin dielectric, h-BN [23]. Excitation with circular-polarized light in resonance with, e.g., A exciton state will create excitons only in either the K or K' valley. Using linear polarized light one can generate excitons in both valleys, where they will have opposite spin orientations [12]. This is different from standard zinc-blend type semiconductors, where both spin states occur in the same point in $\mathbf{k}$ space. It has been demonstrated [24] that optical excitation with circular-polarized light can be used to control the exciton populations in different valleys.

Bose-Einstein condensates (BECs) are many-particle systems demonstrating quantum phenomena at macroscopic level, which are determined by the microscopic interparticle interactions. The adjustability of these interactions is important for the understanding of the macroscopic properties of such complex systems. The realization of BECs containing two bosonic species of ultracold dilute alkali atomic gases has provided an extraordinary physical scenario to study a range of quantum phenomena [25–28], since magnetic-field induced Feshbach resonances provide a tunable interaction between different types of atoms within two-species BECs, which can be made either positive or negative [29,30]. This effect allows for the control of phase separation [28] in such BECs as well as for the study of a number of interesting quantum phenomena, such as the miscibility of superfluids [25], the superfluid-to-Mott-insulator transition [26], and glassy phases in bosonic mixtures [31]. Some similar effects can also occur in so-called spinor BECs where an external magnetic field can lead to the formation of (interacting) spin domains within the condensate [32].

As far as exciton-polariton BECs are concerned, in principle, similar quantum systems can be realized by designing appropriate heterostructures and excitation conditions. Exciton polaritons possess the distinctive spin-polarization degree of freedom (spin of the exciton and polarization of the coupled photon) [5] which has been revealed in experiments demonstrating ballistic propagation of the excited polaritons accompanied by polarization beats due to redistribution of the emission intensity between two crossed polarizations [33] and the optical spin Hall effect, which consists of separation of differently polarized polaritons both in real space and momentum space [34]. Recently, spontaneous symmetry-breaking bifurcations in the polarization state of two-component exciton-polariton condensates were demonstrated [35]. Here one can also expect spinor BECs with an interplay between spin-dependent dynamics and Bose-Einstein condensation [5] and distinct Bogolyubov-type elementary excitations [36], experimental studies of which could be performed at much higher temperatures compared to atomic condensates. Yet, exciton-polariton systems with two possible polarization projections onto the growth axis of the hosting semiconductor heterostructure cannot be considered as strictly two-species condensates because of the presence of a

spin-flipping exciton-exciton scattering [37]. In this respect a structure composed of MX_2 layers placed in a planar microcavity could provide interesting possibilities for studying the MC exciton polaritons. First, as mentioned above, the spin-flipping exciton-exciton scattering should be improbable by virtue of the specific band structure of these materials. Secondly, it seems to be suitable for studying interactions between two distinct Bose-Einstein condensates by creating them in two nearby *identical* 2DSC layers separated by a precisely controlled distance (using an atomic-thin dielectric layer).

In this paper we present calculated results for dispersion curves, mode lifetimes, Rabi splittings, and Hopfield coefficients for such structures with the purpose to stimulate experiments in this direction. We also derive a system of coupled Gross-Pitaevskii equations for a structure consisting of two parallel 2DSC sheets in a microcavity and evaluate the separation-dependent cross-interaction for such a system. In the following two sections we describe the linear properties of the exciton polaritons in a microcavity with one and two MX_2 layers. Section IV is devoted to the nonlinear regime due to polariton-polariton interaction owing to the exciton-exciton coupling within and across the layers, and we conclude in Sec. V.

II. EXCITON-POLARITON DISPERSION CURVES

A. Microcavity with one 2DSC sheet

First we consider the case of one 2DSC sheet placed in the symmetry plane of a Fabry-Perot microcavity [see Fig. 1(a)].

For an empty ideal microcavity of width L, the Fabry-Perot modes are given by [1]

$$\omega_{ph}^{(j)} = \frac{c}{n_c}\sqrt{\left(\frac{\pi}{L}j\right)^2 + k_\perp^2} \approx \frac{c\pi}{n_c L}j + \frac{\hbar k_\perp^2}{2m_{ph}^{(j)}},$$
$$j = 1,2,\ldots, \tag{4}$$

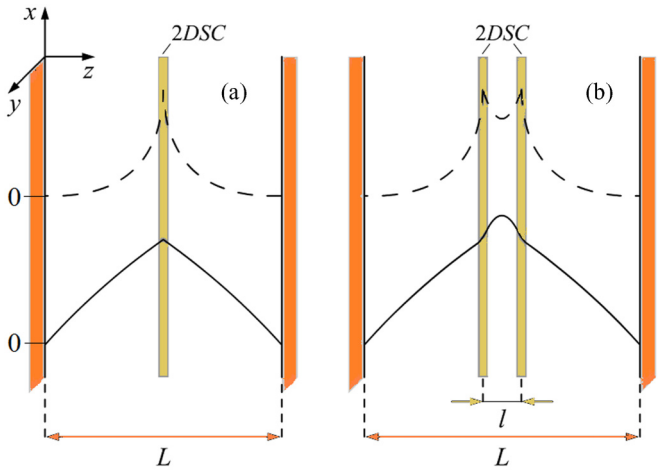

FIG. 1. (Color online) Schematics of a Fabry-Perot microcavity containing one (a) or two (b) nearly 2D semiconductor layers. Qualitative electric field profiles (E_y component) are shown for lowest-order symmetric TE modes, both "bulk" (full curves) and surface (dashed curves). In (b) it is assumed that the space between two layers is filled with a material with a dielectric constant $\varepsilon_2 > \varepsilon$.

where $\mathbf{k}_\perp$ is the in-plane wave vector, $m_{ph}^{(j)} = \frac{\pi n_c \hbar}{cL} j$ is the "photon mass," and $n_c = \sqrt{\varepsilon}$ is the refractive index of the medium filling the cavity. Excitons are confined in the 2DSC layer and can be considered here as perfectly two dimensional, i.e., $\Psi_{ex}(\mathbf{r},z) \sim \Psi_{ex}^{2D}(\mathbf{r})\delta(z - L/2)$, because the microcavity width is much larger than the atomic monolayer thickness. The system possesses translation symmetry in the x-y plane and $\mathbf{k}_\perp$ can be identified with $\mathbf{q}$, the exciton center of mass wave vector. We choose the x axis along $\mathbf{q}$ [see Fig. 1(a)].

To a first approximation, the 2D optical conductivity of a MX_2 layer taking into account the interaction of light with the lowest energy A and B excitons can be written in the form [38]:

$$\sigma_{2D}(\omega,q) = \frac{4e^2v^2}{\pi a_{ex}^2 \omega}\sum_{A,B}\frac{-i}{E_{A,B} + \hbar^2q^2/(2m_{ex}) - \hbar\omega - i\hbar\gamma_{A,B}}, \tag{5}$$

where a_{ex} and m_{ex} are the exciton Bohr radius and mass, respectively, taken as equal for A and B excitons, that can be considered as experimentally obtainable parameters ($a_{ex} \approx$ 0.7–1 nm and $m_{ex} \approx 0.8$–$0.9m_0$ for MoS_2) [15,16], as well as the exciton energies E_A and E_B. The damping parameters γ_A and γ_B can be rather different, as seems to be the case for WS_2 [18]. Equation (5) includes the contributions of two valleys (or, equivalently, two spin projections) for each type of exciton. With the light linearly polarized in the x-y plane, half of the excitons are created in the K valley and the other half in the K' valley (with the opposite spin orientation).

We shall consider both TE (s polarization) and TM waves (p polarization). The uncoupled MC modes can be classified with respect to their parity, and only even modes couple to the 2DSC excitons in the case of Fig. 1(a). For TE waves, the electric field has the only E_y component, and its dependence on x and z for even modes can be written as follows:

$$E_y = \sin(k_z z)e^{iqx}, \quad z \leqslant L/2, \tag{6}$$

$$E_y = \sin[k_z(L - z)]e^{iqx}, \quad z \geqslant L/2, \tag{7}$$

where we have assumed that MC mirrors are perfect. Here

$$k_z = \sqrt{\varepsilon\frac{\omega^2}{c^2} - q^2}. \tag{8}$$

The transverse electric field is continuous at $z = L/2$, which has been taken into account in (7), while the magnetic field component H_x, proportional to the derivative of E_y with respect to z is discontinuous and the boundary condition reads [39]:

$$H_x|_{z=\frac{L}{2}+0} - H_x|_{z=\frac{L}{2}-0} = \frac{4\pi\sigma_{2D}}{c}E_y. \tag{9}$$

Similarly, for TM waves, the magnetic field has only one nonzero component, H_y:

$$H_y = -\cos(k_z z)e^{iqx}, \quad z \leqslant L/2, \tag{10}$$

$$H_y = \cos[k_z(L - z)]e^{iqx}, \quad z \geqslant L/2. \tag{11}$$

The boundary condition (9) holds here with the replacement $H_x \to H_y$ and $E_y \to E_x$, and the latter is continuous.

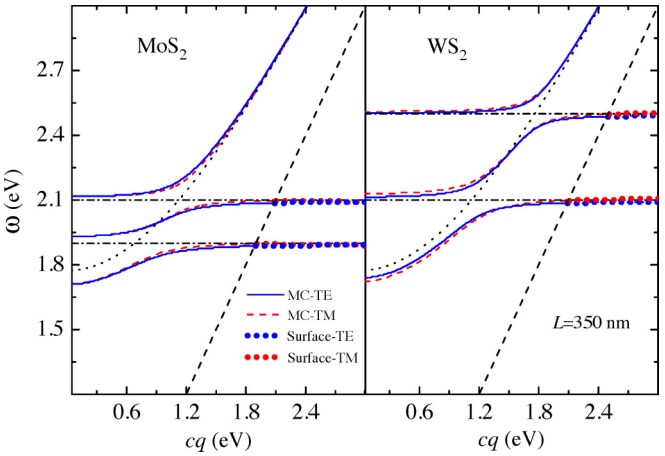

FIG. 2. (Color online) Exciton-polariton dispersion relations for a microcavity of width $L = 350$ nm containing one 2DSC layer: Left panel: MoS_2, right panel: WS_2. TE and TM modes are represented by solid (blue) and dashed (red) curves, respectively. Dash-dotted (dotted) lines correspond to bare excitons [MC photons, Eq. (4)]. Symbols are the surface modes. Straight dashed line is the light line.

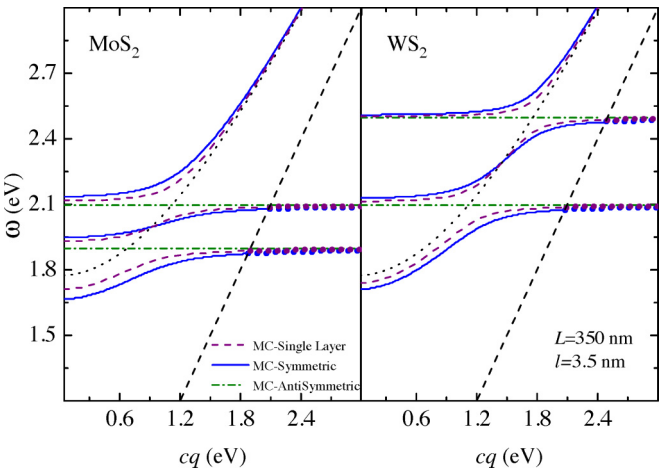

FIG. 3. (Color online) The same as Fig. 2 for TE waves in a microcavity containing two 2DSC layers separated by a distance $l = 3.5$ nm. The symmetric and antisymmetric modes are represented by blue solid and purple dash-dotted lines, respectively. Dashed curves: TE modes for a MC with a single layer. We assumed $\varepsilon = 1$ everywhere in the cavity.

Applying the boundary conditions (which are written explicitly in the Appendix), the exciton-polariton dispersion relations for the TE and TM modes are obtained from the following equations, respectively:

$$\tilde{k}_z \mathrm{Cot}\tilde{k}_z = \frac{\pi\omega L}{c}\tilde{\chi}_{2D}(\omega,q), \tag{12}$$

$$\frac{\mathrm{Cot}\tilde{k}_z}{\tilde{k}_z} = \frac{4\pi c}{\varepsilon\omega L}\tilde{\chi}_{2D}(\omega,q), \tag{13}$$

where we have introduced a dimensionless susceptibility, $\tilde{\chi}_{2D} = i\sigma_{2D}/c$, and wave vector $\tilde{k}_z = \frac{1}{2}k_z L$. The dispersion curves for a microcavity of width $L = 350$ nm (with $\varepsilon = 1$) containing a MoS_2 or WS_2 layer are shown in Fig. 2 (as usual, the damping parameters were put equal to zero). In the calculations we employed the following data for MoS_2 [WS_2]: $E_A = 1.9$ [2.1] eV, $E_B = 2.1$ [2.5] eV, $v = 5.5$ [6.9] $\times 10^7$ cm/s, $a_{ex} = 0.8$ [1.0] nm.

Notice that on the right of the light line, $q = n_c\frac{\omega}{c}$, the wave-vector component along z becomes imaginary and Eqs. (12) and (13) describe states with the fields decreasing exponentially with the distance at both sides of the 2DSC layer. While such modes are common in p polarization, their existence in s polarization is specific for nearly 2D polarizable systems such as graphene where TE plasmon polaritons can exist [39]. In fact, they are the limiting case of guided waves in such an ultimate thin waveguide. We shall call these excitations *surface modes* in order to distinguish them from "bulk" ones (with real k_z), which will be referred to as simply MC exciton polaritons.

B. Microcavity with two 2DSC sheets

Now we will consider the case of two 2DSC layers separated by a distance l, placed symmetrically in the microcavity of width L [see Fig. 1(b)]. As we saw in the previous section, the dispersion curves of TE and TM waves are rather similar, so here we will focus only on the TE modes. We can anticipate that for each mode of the system with one 2DSC layer considered above, there will be two modes, one symmetric and one antisymmetric. Therefore we can choose the solutions for E_y in the different MC regions according to this symmetry. Following the same procedure of the previous section (see Appendix for details), we find that the symmetric modes are governed by the equation:

$$\tilde{k}_z\{\mathrm{Cot}[(1-\alpha)\tilde{k}_z] - \mathrm{Tan}[\alpha\tilde{k}_z]\} = \frac{\pi\omega L}{c}\tilde{\chi}_{2D}(\omega,q) \tag{14}$$

with $\alpha = \frac{l}{L}$. The corresponding equation for the antisymmetric modes reads:

$$\tilde{k}_z\{\mathrm{Cot}[(1-\alpha)\tilde{k}_z] + \mathrm{Cot}[\alpha\tilde{k}_z]\} = \frac{\pi\omega L}{c}\tilde{\chi}_{2D}(\omega,q). \tag{15}$$

The dispersion curves determined by Eqs. (14) and (15) are shown in Fig. 3. While the symmetric (S) modes are qualitatively similar to those of one-2DSC-layer structure, the antisymmetric (AS) modes are almost dispersionless with the frequency almost coinciding with that of the corresponding uncoupled exciton (A or B).

Taking as reference the MC of Fig. 3, the overall splitting $\Delta_{31}(q)$ between the upper and lower branches with frequencies $\omega_3(q)$ (mode 3, B-exciton-like for $q \to 0$ and photonlike for $cq \gtrsim 2$) and $\omega_1(q)$ (mode 1, photonlike for $q \to 0$ and A-exciton-like if $cq \gtrsim 1.8$), respectively, is shown in Fig. 4 for several microcavities with ratio $\alpha = 0.01, 0.1, 0.3, 0.5,$ and 0.7. From the figure it can be seen that (i) the frequency splitting shows a minimum at certain $q = q_{\min}$, which depend on the ratio α, and (ii) the value of $\Delta\omega(q_{\min})$ decreases as α increases. Also, the splitting between the S and AS modes increases for smaller interlayer distances (not shown), however, we found that it almost saturates for $\alpha \leqslant 0.1$.

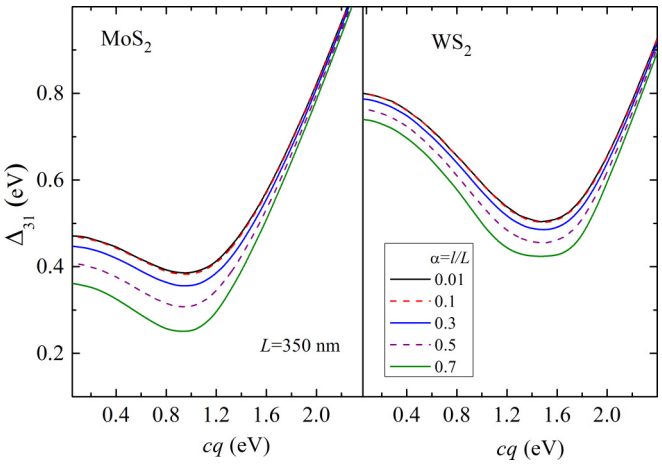

FIG. 4. (Color online) Overall frequency splitting $\Delta_{31} = \omega_3 - \omega_1$ versus q between the uppermost, ω_3, and the lowest, ω_1, exciton-polariton symmetric branches of Fig. 3 for several values of the ratio $\alpha = l/L$.

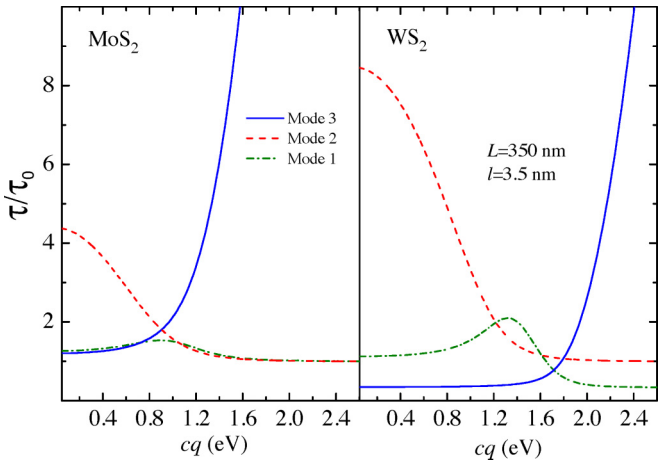

FIG. 5. (Color online) Calculated lifetimes (in units of $\tau_0 = \gamma_A^{-1}$) for three lowest exciton-polariton modes in a MC containing two 2DSC layers. In the calculation we chose $\hbar\gamma_A = 0.00001$ eV corresponding to the *exciton* radiative lifetime of 70 ps.

III. LIFETIME, RABI SPLITTING, AND HOPFIELD COEFFICIENTS

A. Exciton-polariton lifetime

So far, we solved Eqs. (12), (13), (14), and (15) neglecting the imaginary part of $\tilde{\chi}_{2D}$ that yielded the dispersion curves shown in Figs. 2 and 3. Now let us consider the same equations keeping the imaginary part. Each of them links three parameters: ω, q, and k_z. In Eq. (8) we set q as a real independent parameter, therefore we have four equations for the real and imaginary parts of ω and k_z. The inverse of the imaginary part of ω is the exciton-polariton lifetime, which we shall denote by τ. For the case of one 2DSC layer, assuming that $\Im\omega \ll \Re\omega$, the following simple formula can be derived for the lowest order mode:

$$\tau = \gamma_A^{-1}\left(1 + \frac{\pi L \omega_{\mathrm{LT}}}{c}\right), \tag{16}$$

where

$$\omega_{\mathrm{LT}} = \frac{4e^2 v^2}{\pi a_{ex}^2 c E_A} \tag{17}$$

is the oscillator strength of the exciton transition, also known as the longitudinal-transverse exciton splitting [1]. According to Eq. (16), the exciton-polariton lifetime is higher than that of pure exciton ($\tau_0 = \gamma_A^{-1}$). This is also demonstrated, in the case of two layers, by the results of numerical solution of the dispersion approximations, shown in Fig. 5. We see that for the photonlike mode 3 the lifetime tends to infinity, because pure photons do not decay or escape from the microcavity in our model. In contrast, for the case of MoS_2 the middle branch in Fig. 3 (B-exciton-like if $cq > 1.8$ eV, mode 2) is essentially a bare exciton [see Fig. 7(b) below where a discussion of the Hopfield coefficients is given] and the lifetime is almost equal to τ_0. In the case of WS_2 we observe a maximum near $cq = 1.4$ eV, which is explained by the fact that the mode 2 presents a stronger coupling to the electromagnetic field [see Fig. 7(b), right panel].

B. Rabi splitting and Hopfield coefficients

Rabi splitting (RS) is a measure of strength of the coupling between the exciton and the microcavity modes [1]. In our case its definition is not straightforward because there are two anticrossings not far from each other (see Figs. 2 and 3), and all three oscillators are coupled, at least, in a certain range of q. In Fig. 6 we present the minimum values of the splittings, Δ_{31} (whose q dependence is shown in Fig. 4) and $\Delta_{21} = \omega_2 - \omega_1$. The latter can be considered as the Rabi splitting in a common sense (minimum separation between two lowest energy polariton features observed experimentally). For the MC width $L = 350$ nm (corresponding to a detuning of -126 meV with respect to A exciton for MoS_2) the RS value is $\Delta_{21}^{\min} \approx 0.16$ eV for both MoS_2 and WS_2 (see Fig. 6), which is comparable to traditional QWs placed in a semiconductor microcavity. [1] In earlier experimental work on exciton polaritons in a MC with an embedded MoS_2 layer [21], a Rabi splitting of ≈ 50 meV was reported for a smaller detuning of -40 meV. Our calculations for that case (taking $\varepsilon = 2$ and $L = 236$ nm yields a -40 meV detuning) give $\Delta_{21}^{\min} \approx 0.16$ eV. This approximately 2.5-fold discrepancy can be partially understood because of the nonideality of the real microcavity and can also be explained by uncertainty of the input parameters. For instance, considerably larger values of the exciton Bohr radius ($a_{ex} = 1.35$ nm for A excitons in MoS_2) have been suggested in the literature [40]. If we used this value as an input parameter, the splitting would be decreased by a factor of two. Finally, we would like to point out that for structures with two 2DSC layers, RS can be modulated by $\pm 30\%$ by varying the separation between the layers (see Fig. 6).

Now we proceed to the quantum-mechanical description of the exciton polaritons. Let us consider a microcavity with one 2DSC layer. The Hamiltonian describing the interaction of A and B excitons with cavity photons reads:

$$H = \sum_{\mathbf{q}} \left[E_c(\mathbf{q}) P_{\mathbf{q}}^{\dagger} P_{\mathbf{q}} + E_A(\mathbf{q}) A_{\mathbf{q}}^{\dagger} A_{\mathbf{q}} + E_B(\mathbf{q}) B_{\mathbf{q}}^{\dagger} B_{\mathbf{q}} + g_{A\text{-}ph}(\mathbf{q}) P_{\mathbf{q}}^{\dagger} A_{\mathbf{q}} + g_{B\text{-}ph}(\mathbf{q}) P_{\mathbf{q}}^{\dagger} B_{\mathbf{q}} + \mathrm{H.c.}\right], \tag{18}$$

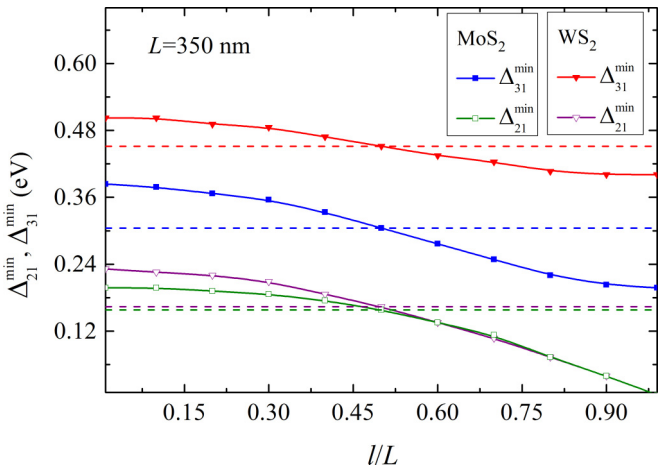

FIG. 6. (Color online) Minimal mode separations Δ_{31} (overall splitting) and Δ_{21} (Rabi splitting for A exciton polaritons neglecting B excitons) vs distance between two 2DSC layers. Dashed lines indicate the corresponding values for one 2DSC layer placed in the MC symmetry plane.

where $A_{\mathbf{q}}(A_{\mathbf{q}}^{\dagger})$, $B_{\mathbf{q}}(B_{\mathbf{q}}^{\dagger})$, and $P_{\mathbf{q}}(P_{\mathbf{q}}^{\dagger})$ are annihilation (creation) operators for the two types of excitons and the cavity photons, respectively, and $E_{A}(\mathbf{q}), E_{B}(\mathbf{q})$ and $E_c(\mathbf{q})$ are the energies of the decoupled excitons and photons. The photon-exciton interaction energies are represented by $g_{A\text{-}ph}(\mathbf{q})$ and $g_{B\text{-}ph}(\mathbf{q})$. We include into consideration only the lowest MC mode with $j = 1$, because the other modes have much higher energies and nearly do not interact with the A and B exciton states.

The Hamiltonian (18) is diagonalized by using the polaritonic basis with the unitary transformation [41]

$$\alpha_{\mathbf{q}}^{(i)} = \kappa_{ph}^{(i)}(\mathbf{q})P_{\mathbf{q}} + \kappa_{B}^{(i)}(\mathbf{q})B_{\mathbf{q}} + \kappa_{A}^{(i)}(\mathbf{q})A_{\mathbf{q}}, \quad i = 1, 2, 3, \tag{19}$$

where $\alpha_{\mathbf{q}}^{(i)}$ are the annihilation operators for exciton polaritons of three branches (which will be labeled by $i = 1, 2, 3$) and $\kappa_{j,}^{(i)}$ $(j = 1_{ph}, A, B)$ are the Hopfield coefficients (HC). [1] The quantity $(\kappa_{j}^{(i)})^2$ represents the contribution of the exciton, A or B, or the photon mode 1 to the polariton mode i. The first two of them determine the polariton-polariton interaction, which occurs through the excitonic part of these composite excitations and will be considered in the next section. The Hopfield coefficients fulfill the normalization condition,

$$\left(\kappa_{ph}^{(i)}(\mathbf{q})\right)^2 + \left(\kappa_{B}^{(i)}(\mathbf{q})\right)^2 + \left(\kappa_{A}^{(i)}(\mathbf{q})\right)^2 = 1. \tag{20}$$

The transformation matrix of Eq. (19) can be expressed through the eigenvectors of the Hamiltonian (18), and its columns are orthogonal. Together with the normalization conditions (20), there are six relations for the coefficients $\kappa_{j}^{(i)}$, i.e., only three of them are independent (for each $\mathbf{q}$). We can use the polariton dispersion curves calculated in the previous section (plus those of bare excitons and MC photons) to determine these coefficients, thus avoiding an explicit definition of the interaction parameters $g_{A\text{-}ph}$, etc. and achieving the correspondence between the quasiclassical and quantum-mechanical pictures.

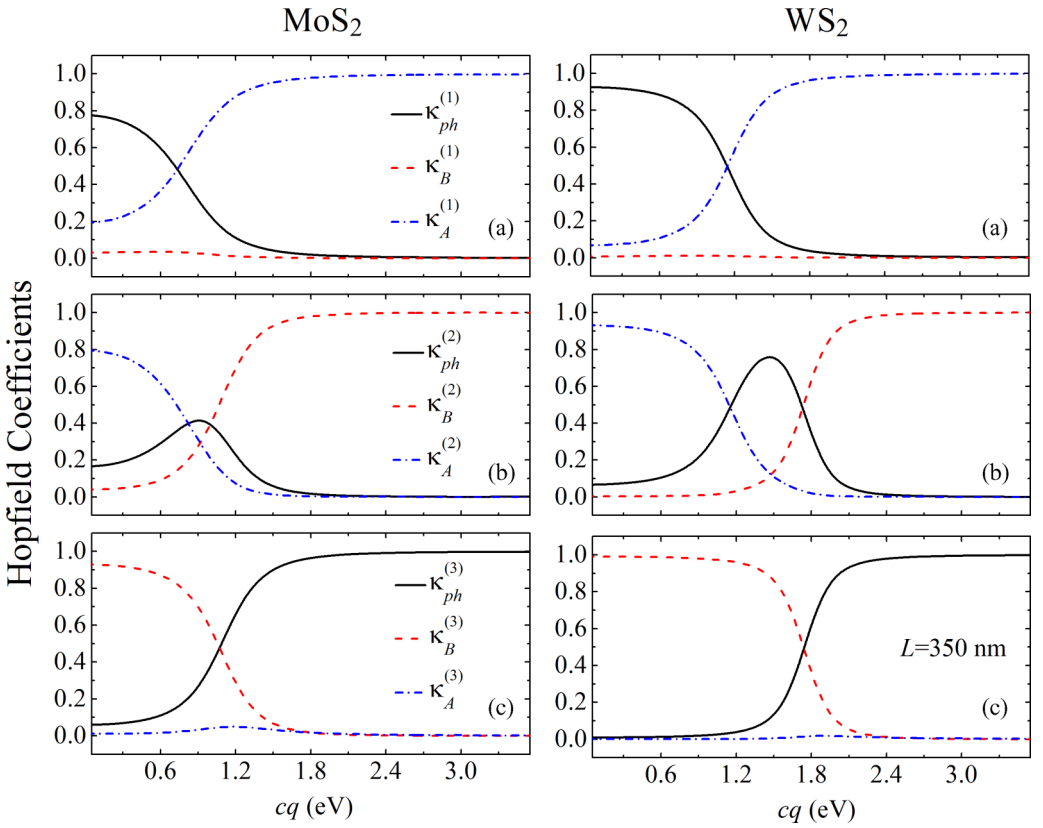

FIG. 7. (Color online) Hopfield coefficients for exciton polaritons in a microcavity with one 2DSC layer placed in the symmetry plane.

The solution for the HCs is given by:

$$\kappa_{ph}^{(i)}(q) = \frac{\Delta_A^{(i)}(q)\Delta_B^{(i)}(q)}{\sqrt{\Delta_A^{(i)2}(q)\Delta_B^{(i)2}(q) + \Delta_B^{(i)2}(q)g_{A\text{-}ph}^2(q) + \Delta_A^{(i)2}(q)g_{B\text{-}ph}^2(q)}},$$

$$\kappa_A^{(i)}(q) = -\frac{\Delta_B^{(i)}(q)g_{A\text{-}ph}(q)}{\sqrt{\Delta_A^{(i)2}(q)\Delta_B^{(i)2}(q) + \Delta_B^{(i)2}(q)g_{A\text{-}ph}^2(q) + \Delta_A^{(i)2}(q)g_{B\text{-}ph}^2(q)}},$$

$$\kappa_B^{(i)}(q) = -\frac{\Delta_A^{(i)}(q)g_{B\text{-}ph}(q)}{\sqrt{\Delta_A^{(i)2}(q)\Delta_B^{(i)2}(q) + \Delta_B^{(i)2}(q)g_{A\text{-}ph}^2(q) + \Delta_A^{2(i)}(q)g_{B\text{-}ph}^2(q)}}, \quad (21)$$

where $\Delta_{A,B}^{(i)}(q) = E_{A,B} - E_i$ is the energy difference between the exciton A, B, and the ith polariton mode (notice that the system is isotropic in the x-y plane). The exciton-photon interaction parameters are expressed through the energies of the coupled and uncoupled modes as follows [42]:

$$g_{A\text{-}ph}^2(q) = \Delta_A^{(1)}(q)\Delta_A^{(2)}(q)\frac{\Delta_B^{(1)}(q)[E_c(q) - E_1(q)] - \Delta_B^{(2)}(q)[E_c(q) - E_2(q)]}{\Delta_B^{(1)}(q)\Delta_A^{(2)}(q) - \Delta_B^{(2)}(q)\Delta_A^{(1)}(q)}, \quad (22)$$

and $g_{B\text{-}ph}^2$ is obtained from Eq. (22) by permutating the indices A and B. The q dependence of the Hopfield coefficients for the present case is shown in Fig. 7. It can be observed that the lowest exciton-polariton mode is practically uncoupled from the B exciton for both materials. Exactly at the crossing point ($cq \approx 0.85$ eV for MoS_2) these polaritons are half photons, half A excitons, while for larger q they become nearly bare A excitons. It means that one can disregard B excitons when focusing on this polariton branch, which would simplify the analysis. We notice that the values and the q dependence of the coefficients $\kappa_A^{(1)}$ and $\kappa_{ph}^{(1)}$ for MoS_2 are quite similar to those extracted from the experimentally measured angle-resolved reflectivity spectra [21]. The second polariton branch [Fig. 7(b)] is mostly a composition of A and B excitons, with an admixture of photons near the crossing point, and the third branch [Fig. 7(c)] is photonlike for large wave vectors. The Hopfield coefficients will be used in the next section to determine the polariton-polariton interaction parameters in the high excitation regime.

IV. NONLINEAR REGIME

Bose-Einstein condensates of exciton polaritons have been experimentally realized in semiconductor microcavities (see Refs. [8–10]). The theoretical description of their dynamics is based on the Gross-Pitaevskii (GP) equation [43], which can be derived from the following many-body Hamiltonian [44]:

$$\mathcal{H} = \int d\mathbf{r}\hat{\Psi}^\dagger(\mathbf{r})\left[-\frac{\hbar^2}{2m_p}\nabla_{\mathbf{r}}^2 + V_c\right]\Psi(\mathbf{r}) + \frac{1}{2}\int d\mathbf{r}d\mathbf{r}'\hat{\Psi}^\dagger(\mathbf{r})\hat{\Psi}^\dagger(\mathbf{r}')V(\mathbf{r}-\mathbf{r}')\hat{\Psi}(\mathbf{r})\hat{\Psi}(\mathbf{r}'), \quad (23)$$

where m_p is the polariton mass (which is determined by the second derivative of the polariton dispersion curve at $q = 0$), $V_c(\mathbf{r})$ is a confinement potential, and $V(\mathbf{r} - \mathbf{r}')$ describes two-particle interactions. In the standard procedure one assumes that the operator $\hat{\Psi}(\mathbf{r},t)$ can be approximated by its expectation value $\Phi(\mathbf{r},t)$, and the two-particle potential is approximated by a δ function $V(\mathbf{r} - \mathbf{r}') = \Lambda\delta(\mathbf{r} - \mathbf{r}')$, which yields the GP equation with Λ denoting the particle-particle self-interaction parameter [44]. In our case $\mathbf{r}$ should be considered as a two-dimensional vector in the x-y plane.

The polariton-polariton interaction potential is the exciton-exciton coupling renormalized due to the change of the basis (from excitons and photons to polaritons), projected onto the polariton branch i which we are interested in. It can be shown (see, e.g., Ref. [45]) that the renormalization involves an integral of the form:

$$\frac{1}{(2\pi)^4}\int d\mathbf{r}''d\mathbf{r}'''\int d\mathbf{k_1}d\mathbf{k_2}d\mathbf{q}\tilde{V}^{ex-ex}(\mathbf{q})\kappa_{ex}^{(i)}(\mathbf{k_1})^\star\kappa_{ex}^{(i)}(\mathbf{k_2})^\star \times \kappa_{ex}^{(i)}(\mathbf{k_1}-\mathbf{q})\kappa_{ex}^{(i)}(\mathbf{k_2}+\mathbf{q}) \times \exp\{i[\mathbf{q}(\mathbf{r}''-\mathbf{r}''') + \mathbf{k_1}(\mathbf{r}-\mathbf{r}'') + \mathbf{k_2}(\mathbf{r}'-\mathbf{r}''')]\},$$

where $\mathbf{r}''$, $\mathbf{r}'''$, and all wave vectors are two dimensional, and $\tilde{V}^{ex-ex}(\mathbf{q})$ is the Fourier transform of the exciton-exciton interaction potential; here $ex = A$ or B. The Hopfield coefficients are almost independent of the wave vector when its modulus is relatively small (see Fig. 7), so the usual approximation [1,45,46] is to replace all four of them in the above integral by $X \equiv \kappa_{ex}^{(i)}(0)$, which yields a dramatic simplification,

$$V(\mathbf{r}-\mathbf{r}') = |X|^4\int d\mathbf{q}\tilde{V}^{ex-ex}(\mathbf{q})e^{i\mathbf{q}(\mathbf{r}-\mathbf{r}')}. \quad (24)$$

If $\tilde{V}^{ex-ex}(\mathbf{q})$ only weakly depends on $\mathbf{q}$, the integral in Eq. (24) gives a δ function, and thus the necessary step for obtaining the GP equation is justified.

Under excitation with a circular-polarized light, all the A-type excitons have the same spin polarization, and their condensate can be described by a scalar order parameter. The particle-particle interaction within such a condensate is due to both Coulomb and exchange interaction between the excitons with parallel spins, which has been considered in a number of works [37,47] showing that indeed $\tilde{V}^{ex-ex}(\mathbf{q}) \approx const$ for $qa_{ex} \ll 1$, and the polariton-polariton interaction parameter can be approximated as [47]

$$\Lambda = 6R_A a_{ex}^2|X|^4, \quad (25)$$

where R_A is the A-exciton Rydberg constant [48]. Linear-polarized light can be considered as a superposition of left-hand and right-hand polarized photons and, theoretically, can create a condensate consisting of two differently polarized polariton species within a 2DSC layer. Such condensates are described by a spinor order parameter [5],

$$\Phi(\mathbf{r},t)=\begin{bmatrix}\Phi_1(\mathbf{r},t)\\ \Phi_2(\mathbf{r},t)\end{bmatrix}. \tag{26}$$

Its components obey a system of two coupled GP equations:

$$i\hbar\frac{\partial}{\partial t}\Phi(\mathbf{r},t)=\mathbf{L}\Phi(\mathbf{r},t), \tag{27}$$

where $\mathbf{L}$ is a 2×2 nonlinear operator given by

$$\mathbf{L}=\begin{bmatrix}-\frac{\hbar^2}{2m_p}\nabla_{\mathbf{r}}^2+V_c+\Lambda|\Phi_1|^2 & \Lambda_{12}\Phi_1\Phi_2^\star\\ \Lambda_{21}\Phi_1^\star\Phi_2 & -\frac{\hbar^2}{2m_p}\nabla_{\mathbf{r}}^2+V_c+\Lambda|\Phi_2|^2\end{bmatrix}. \tag{28}$$

Here $\Lambda_{12}=\Lambda_{21}^\star$ is a parameter representing the interaction of excitons with opposite spins.

As mentioned above, excitons with different spin polarizations occupy different valleys in the Brillouin zone of the 2DSC material, so there is no particle exchange between two subsystems and each component Φ_i satisfies a separate normalization condition,

$$\int|\Phi_i(\mathbf{r},t)|=N_i,\quad i=1,2,$$

where N_i denotes the number of polaritons in the ith condensate. Usually for QW excitons the interaction is much stronger for parallel spins [5,45], so one can expect $|\Lambda_{12}|\ll\Lambda$ and a rather weak coupling between two BECs. However, some further mechanisms can operate. As known, the orientation of the condensate polarization can be pinned along one of the crystallographic axes of the sample, which manifests a difference between two perpendicular directions in the x-y plane and can be due to some anisotropy in the microcavity [5]. Such a condensate with a certain polarization state can be characterized by a scalar order parameter and an effective interaction parameter (a combination of Λ and Λ_{12}) [49].

Let us consider now two 2DSC layers in a microcavity, as shown in Fig. 1(b), where it is possible to create two condensates (one in each 2DSC layer) separated by a distance l. Its many-body Hamiltonian can be written as

$$\mathcal{H}_2=\sum_{i=1,2}\mathcal{H}^{(i)}+\frac{1}{2}\int d\mathbf{r_1}d\mathbf{r_2}\hat\Psi_1^\dagger(\mathbf{r_1})\hat\Psi_2^\dagger(\mathbf{r_2})V_{12}\times(\mathbf{r_1}-\mathbf{r_2}-l\mathbf{e}_z)\hat\Psi_1(\mathbf{r_1})\hat\Psi_2(\mathbf{r_2}), \tag{29}$$

where $\mathcal{H}^{(i)}$ is given by Eq. (23) and V_{12} describes the interaction between two different condensates (we shall consider each of them as scalar for simplicity). In the mean field approximation, neglecting the q dependence of the Hopfield coefficients, the last term in Eq. (29) can be written as

$$U_{12}=\frac{1}{2}|X|^4\int d\mathbf{r_1}d\mathbf{r_2}|\Phi_1(\mathbf{r_1})|^2V_{12}^{ex-ex}\times(\mathbf{r_1}-\mathbf{r_2}-l\mathbf{e}_z)|\Phi_2(\mathbf{r_2})|^2, \tag{30}$$

where $\tilde V_{12}(\mathbf{r_1}-\mathbf{r_2}-l\mathbf{e}_z)$ is the exciton-exciton interaction potential between different 2DSC sheets, and the Hopfield coefficients have been assumed to be the same for both condensates. The coupling between the condensates located in different 2DSC sheets takes place due to the electromagnetic interaction between the excitons. It is mediated by transient dipoles associated with resonant exciton transitions and is similar to the Förster resonant energy transfer process (FRET) [50]. The energy of the dipole-dipole interaction between two excitons separated by a radius vector $\mathbf{R}=\mathbf{r_1}-\mathbf{r_2}-l\mathbf{e}_z$ is [50]

$$V_{12}^{ex-ex}(\mathbf{R})=\frac{\mu_1\cdot\mu_2-3(\mu_1\cdot\mathbf{e_R})(\mu_2\cdot\mathbf{e_R})}{\varepsilon R^3}, \tag{31}$$

where μ_i denotes the dipole moment of the exciton located in the sheet $i=1,2$, and $\mathbf{e_R}=\mathbf{R}/R$. It has to be averaged over all possible orientations of $\mu_{1,2}$ in the x-y plane, therefore, if the dipoles are uncorrelated, the averaging will yield zero, and there is no direct Coulomb interaction between the condensates. However, if we consider $\mu_{1,2}$ as transient dipoles due to exciton transitions coupled to the MC field, they will be the same for a symmetric MC mode, since the considered structure is symmetric with respect to the plane $z=L/2$. If we consider a TE mode, the electric field has only a y component, and we have

$$\mu_{1x}=\mu_{2x}=0,$$
$$\mu_{1y}=\mu_{2y}=\alpha E_y^0|_{z=\frac{L}{2}\pm\frac{l}{2}},$$

where α is the exciton polarizability and E_y^0 denotes the electric field in *empty* microcavity. In analogy with a quantum dot, the exciton polarizability can be written as [51]

$$\alpha(\omega)=\tilde\chi_{2D}(\omega)a_{ex}^2b_0, \tag{32}$$

where b_0 is the exciton extension along z (of the order of the 2DSC layer thickness). Therefore we can write:

$$\langle\mu_1\cdot\mu_2\rangle=\left(\alpha E_y^0|_{z=L/2\pm l/2}\right)^2.$$

Therefore the intercondensate interaction energy is written as

$$U_{12}=\frac{1}{2}\left(\alpha E_y^0|_{z=L/2\pm l/2}\right)^2|X|^4\int d\mathbf{r_1}|\Phi_1(\mathbf{r_1})|^2\times\int d\mathbf{r_2}\mathcal{K}(\mathbf{r_1}-\mathbf{r_2})|\Phi_2(\mathbf{r_2})|^2, \tag{33}$$

with the kernel

$$\mathcal{K}(\mathbf{r_1}-\mathbf{r_2})=\mathcal{K}(r_{12},\phi)=\frac{r_{12}^2(1-3\cos^2\phi)+l^2}{\left(r_{12}^2+l^2\right)^{5/2}}, \tag{34}$$

where ϕ is the angle between $\mathbf{r_{12}}=\mathbf{r_1}-\mathbf{r_2}$ and the y axis. The variation of Eq. (29) with Eq. (33) with respect to Φ_i leads to coupled integrodifferential equations. In order to simplify them to differential GP equations, we shall make the following (rather crude) approximation:

$$\mathcal{K}(\mathbf{r_1}-\mathbf{r_2})\approx\left\{\int d\mathbf{r}\mathcal{K}(\mathbf{r})\right\}\delta_{2D}(\mathbf{r_1}-\mathbf{r_2}), \tag{35}$$

where the term in brackets is the $\mathbf{q}=0$ Fourier component of the kernel and δ_{2D} denotes the 2D Dirac function. The integral

in Eq. (35) is equal to $\frac{4\pi}{15l}$. Thus, Eq. (30) can be written as

$$U_{12} = \frac{2\pi}{15l}|X|^4\left(\alpha E_y^0|_{z=L/2\pm l/2}\right)^2 \int d\mathbf{r}|\Phi_1(\mathbf{r})|^2|\Phi_2(\mathbf{r})|^2, \tag{36}$$

and the system under consideration can be described formally by the same two coupled GP equations (28). The parameter Λ is given by Eq. (25), and the intercondensate interaction constant is

$$\Lambda_{12} = \frac{4\pi}{15l}|X|^4\left(\alpha E_y^0|_{z=L/2\pm l/2}\right)^2. \tag{37}$$

The dependence of Λ_{12} on l (roughly $\sim l^{-1}$ for small l) together with the number of particles N_1 and N_2 in each condensate provide a means to control the coupling effect between the two condensates.

V. CONCLUSION

In summary, we analyzed the properties of exciton polaritons in a Fabry-Perot microcavity containing one or two monolayer-thin semiconductor sheets taking as examples MoS_2 and WS_2 and calculated the dispersion curves, mode lifetimes, Rabi splittings, and Hopfield coefficients. Our results suggest that they are interesting for studying the rich physics associated with the Bose-Einstein condensation of exciton polaritons. Both materials seem appropriate for this purpose; WS_2 may look more attractive because of the larger separation between the A and B excitons and, consequently, easier analysis, however, even for MoS_2 the fraction of B excitons in the lowest polariton branch is rather small. One interesting feature of these materials is the separation of excitons with opposite spins in $\mathbf{k}$ space. If a Bose-Einstein condensate is created involving both spin orientations, it should be called a two-species BEC (similar to cold atom systems [25–28]) rather than a spinor condensate. Maybe it is possible to separately control the number of particles in each subsystem by using an elliptically polarized light.

We also considered polariton properties and derived a system of coupled Gross-Pitaevskii equations for a microcavity containing two condensates localized in different semiconductor sheets. The Rabi splitting in this structure is enhanced, compared to the case of a single semiconductor sheet, for small intersheet distances. It reaches values similar to those characteristic of hybrid organic-inorganic systems with simultaneous coupling of two degenerate excitons and a microcavity photon [52]. The (nonlinear) intercondensate interaction is resonant (similar to FRET) and approximately inversely proportional to the distance separating two sheets. It can be controlled by adjusting this distance with a very high precision by using the atomically thin dielectric h-BN. In principle, it should also be possible to create two condensates independently by using two lasers that should lead to different scenarios governed by the population numbers of both BEC's. It would also open a way of extension of experiments with polariton condensates making use of their interaction with uncondensed polaritons [53,54]. On the theoretical side, the analysis of coupled GP equations (28) with adjustable coupling parameter can yield classes of solutions known in nonlinear optics [55] but so far unexplored in the field of Bose-Einstein condensates.

ACKNOWLEDGMENTS

This work was supported by the CNPq (Brazil) and the FCT (Portugal). M.I.V. wishes to thank Centro Brasileiro de Pesquisas Físicas (Rio de Janeiro, Brazil) for hospitality. M.I.V. and N.M.R.P. acknowledge financial support from the EC Graphene Flagship Project (Contract No. CNECT-ICT-604391). A.K. thanks the EPSRC Established Career Fellowship for financial support.

APPENDIX: POLARITON DISPERSION RELATION FOR MC WITH TWO 2DSC SHEETS

The z coordinates of the 2DSC sheets are $z_{1,2} = (L \mp l)/2$. The system is symmetric with respect to the $z = L/2$ plane, so we can foresee that there are two modes for each polariton mode of the system with one 2DSC sheet, one symmetric and one antisymmetric. Here we shall assume that the dielectric constant of the material filling the regions $0 \leqslant z \leqslant z_1$ and $z_2 \leqslant z \leqslant L$ is ε_1, while the space between the semiconductor layers can be filled with another dielectric with the dielectric constant ε_2.

For TE waves the electric field component is written as follows:

$$\begin{aligned} E_y &= \sin\left(k_z^{(1)}z\right)e^{iqx}, \quad 0 \leqslant z \leqslant z_1, \\ E_y &= \begin{bmatrix} a\cos\left[k_z^{(2)}(z-L/2)\right] \\ b\sin\left[k_z^{(2)}(z-L/2)\right] \end{bmatrix} \times e^{iqx}, z_1 \leqslant z \leqslant z_2, \\ E_y &= \pm\sin\left[k_z^{(1)}(L-z)\right]e^{iqx}, \quad z_2 \leqslant z \leqslant L, \end{aligned} \tag{A1}$$

where the upper (lower) line or sign corresponds to symmetric (antisymmetric) mode, a and b are some constants, and

$$k_z^{(i)} = \sqrt{\varepsilon_i\frac{\omega^2}{c^2} - q^2}, \quad i = 1, 2. \tag{A2}$$

The magnetic field component H_x is obtained from Eq. (A1) through the Maxwell equation $\partial\mathbf{H}/\partial t = -c(\nabla \times \mathbf{E})$. The application of boundary conditions, Eq. (9), and continuity of E_y at $z = z_1$ yields two equations for each case (and boundary conditions at $z = z_2$ are satisfied automatically since the symmetry has been taken into account), from which the constant a or b can be eliminated. Therefore we have, for symmetric modes:

$$\begin{aligned} &\frac{ck_z^{(1)}}{\omega} - \frac{ck_z^{(2)}}{\omega}\tan\left(k_z^{(1)}z_1\right)\tan\left(k_z^{(2)}l/2\right) \\ &\quad = \frac{4\pi i\sigma_{2D}}{c}\tan\left(k_z^{(1)}z_1\right), \end{aligned} \tag{A3}$$

and for antisymmetric modes:

$$\frac{ck_z^{(1)}}{\omega} + \frac{ck_z^{(2)}}{\omega}\tan\left(k_z^{(1)}z_1\right)\cot\left(k_z^{(2)}l/2\right) = \frac{4\pi i\sigma_{2D}}{c}\tan\left(k_z^{(1)}z_1\right). \tag{A4}$$

If we put $k_z^{(1)} = k_z^{(2)}$, Eqs. (A3) and (A4) simplify to Eqs. (14) and (15). For $l \to 0$ the frequency of the symmetric mode tends to that of a MC containing a single 2D semiconductor layer with the optical conductivity $2\sigma_{2D}$, while for the antisymmetric mode we have $\omega \to \omega_0$. The corresponding surface modes are obtained by substituting $k_z^{(i)} = i\kappa_i$ into Eqs. (A3) and (A4).

Considering now TM waves, the magnetic field component is written as

$$H_y = -\cos\left(k_z^{(1)} z\right) e^{iqx}, \quad 0 \leqslant z \leqslant z_1, \quad H_y = \begin{bmatrix} a \sin\left[k_z^{(2)}(z - L/2)\right] \\ b \cos\left[k_z^{(2)}(z - L/2)\right] \end{bmatrix} \times e^{iqx}, \quad z_1 \leqslant z \leqslant z_2,$$

$$H_y = \pm \cos\left[k_z^{(1)}(L - z)\right] e^{iqx}, \quad z_2 \leqslant z \leqslant L, \tag{A5}$$

with the same distinction between symmetric and antisymmetric modes as above. Using boundary conditions for H_y at $z = z_1$,

$$H_y|_{z=z_1+0} - H_y|_{z=z_1-0} = \frac{4\pi i \sigma_{2D}}{\omega} \left(\frac{1}{\varepsilon} \frac{\partial H_y}{\partial z} \right) \Big|_{z=z_1}, \tag{A6}$$

$$\frac{1}{\varepsilon_1} \frac{\partial H_y}{\partial z} \Big|_{z=z_1-0} = \frac{1}{\varepsilon_2} \frac{\partial H_y}{\partial z} \Big|_{z=z_1+0}, \tag{A7}$$

we obtain the following dispersion relations:

$$1 - \frac{\varepsilon_2 k_z^{(1)}}{\varepsilon_1 k_z^{(2)}} \tan\left(k_z^{(1)} z_1\right) \tan\left(k_z^{(2)} l/2\right) = \frac{4\pi i \sigma_{2D} k_z^{(1)}}{\varepsilon_1 \omega} \tan\left(k_z^{(1)} z_1\right) \tag{A8}$$

for the symmetric modes, and

$$1 + \frac{\varepsilon_2 k_z^{(1)}}{\varepsilon_1 k_z^{(2)}} \tan\left(k_z^{(1)} z_1\right) \cot\left(k_z^{(2)} l/2\right) = \frac{4\pi i \sigma_{2D} k_z^{(1)}}{\varepsilon_1 \omega} \tan\left(k_z^{(1)} z_1\right) \tag{A9}$$

for the antisymmetric modes.

[1] A. V. Kavokin, J. J. Baumberg, G. Malpuech, and F. P. Laussy, *Microcavities* (Oxford University Press, Oxford, UK, 2008).
[2] E. M. Purcell, Phys. Rev. **69**, 681 (1946).
[3] O. L. Berman, Y. E. Lozovik, and D. W. Snoke, Phys. Rev. B **77**, 155317 (2008).
[4] H. Deng, H. Haug, and Y. Yamamoto, Rev. Mod. Phys. **82**, 1489 (2010).
[5] I. A. Shelykh, A. V. Kavokin, Y. G. Rubo, T. C. H. Liew, and G. Malpuech, Semicond. Sci. Technol. **25**, 013001 (2010).
[6] G. Christmann, R. Butté, E. Feltin, J.-F. Carlin, and N. Grandjean, Appl. Phys. Lett. **93**, 051102 (2008).
[7] T. C. H. Liew, M. M. Glazov, K. V. Kavokin, I. A. Shelykh, M. A. Kaliteevski, and A. V. Kavokin, Phys. Rev. Lett. **110**, 047402 (2013).
[8] J. Kasprzak, M. Richard, S. Kundermann, A. Baas, P. Jeambrun, J. M. J. Keeling, F. M. Marchetti, M. H. Szymanska, R. André, J. L. Staehli *et al.*, Nature (London) **443**, 409 (2006).
[9] R. Balili, V. Hartwell, D. W. Snoke, L. Pfeiffer, and K. West, Science **316**, 1007 (2007).
[10] A. Amo, D. Sanvitto, F. P. Laussy, D. Ballarini, E. del Valle, M. D. Martin, A. Lemaître, J. Bloch, D. N. Krizhanovskii, M. S. Skolnick *et al.*, Nature (London) **457**, 291 (2009).
[11] L. Britnell, R. M. Ribeiro, A. Eckmann, R. Jalil, B. D. Belle, A. Mishchenko, Y.-J. Kim, R. V. Gorbachev, T. Georgiou, S. V. Morozov *et al.*, Science **340**, 1311 (2013).
[12] M. Palummo, M. Bernardi, and J. C. Grossman, Nano Lett. **15**, 2794 (2015).
[13] F. Wu, F. Qu, and A. H. MacDonald, Phys. Rev. B **91**, 075310 (2015).
[14] D. Xiao, G.-B. Liu, W. Feng, X. Xu, and W. Yao, Phys. Rev. Lett. **108**, 196802 (2012).
[15] R. M. Ribeiro (private communication, 2015).
[16] C. Zhang, H. Wang, W. Chan, C. Manolatou, and F. Rana, Phys. Rev. B **89**, 205436 (2014).
[17] K. He, N. Kumar, L. Zhao, Z. Wang, K. F. Mak, H. Zhao, and J. Shan, Phys. Rev. Lett. **113**, 026803 (2014).
[18] A. Chernikov, T. C. Berkelbach, H. M. Hill, A. Rigosi, Y. Li, O. B. Aslan, D. R. Reichman, M. S. Hybertsen, and T. F. Heinz, Phys. Rev. Lett. **113**, 076802 (2014).
[19] C. Mai, Y. G. Semenov, A. Barrette, Y. Yu, Z. Jin, L. Cao, K. W. Kim, and K. Gundogdu, Phys. Rev. B **90**, 041414 (2014).
[20] M. Koperski, K. Nogajewski, A. Arora, V. Cherkez, P. Mallet, J.-Y. Veuillen, J. Marcus, P. Kossacki, and M. Potemski, Nat. Nanotechnol. **10**, 503 (2015).
[21] X. Liu, T. Galfsky, Z. Sun, F. Xia, E. chen Lin, Y.-H. Lee, S. Kéna-Cohen, and V. M. Menon, Nat. Photon. **9**, 30 (2014).
[22] Y.-C. Lin, C.-Y. S. Chang, R. K. Ghosh, J. Li, H. Zhu, R. Addou, B. Diaconescu, T. Ohta, X. Peng, N. Lu, M. J. Kim, J. T. Robinson, R. M. Wallace, T. S. Mayer, S. Datta, L.-J. Li, and J. A. Robinson, Nano Lett. **14**, 6936 (2014).
[23] A. K. Geim and I. V. Grigorieva, Nature (London) **499**, 419 (2013).
[24] H. Zeng, J. Dai, W. Yao, D. Xiao, and X. Cui, Nat. Nanotechnol. **7**, 490 (2012).
[25] G. Modugno, M. Modugno, F. Riboli, G. Roati, and M. Inguscio, Phys. Rev. Lett. **89**, 190404 (2002).
[26] G. Thalhammer, G. Barontini, L. De Sarlo, J. Catani, F. Minardi, and M. Inguscio, Phys. Rev. Lett. **100**, 210402 (2008).
[27] D. J. McCarron, H. W. Cho, D. L. Jenkin, M. P. Köppinger, and S. L. Cornish, Phys. Rev. A **84**, 011603 (2011).
[28] S. B. Papp, J. M. Pino, and C. E. Wieman, Phys. Rev. Lett. **101**, 040402 (2008).
[29] S. L. Cornish, N. R. Claussen, J. L. Roberts, E. A. Cornell, and C. E. Wieman, Phys. Rev. Lett. **85**, 1795 (2000).
[30] N. R. Claussen, S. J. J. M. F. Kokkelmans, S. T. Thompson, E. A. Donley, E. Hodby, and C. E. Wieman, Phys. Rev. A **67**, 060701 (2003).
[31] T. Roscilde and J. I. Cirac, Phys. Rev. Lett. **98**, 190402 (2007).

[32] J. Stenger, S. Inouye, D. Stamper-Kurn, H.-J. Miesner, A. Chikkatur, and W. Ketterle, Nature (London) **396**, 345 (1998).
[33] W. Langbein, I. Shelykh, D. Solnyshkov, G. Malpuech, Y. Rubo, and A. Kavokin, Phys. Rev. B **75**, 075323 (2007).
[34] C. Leyder, M. Romanelli, J. P. Karr, E. Giacobino, T. C. H. Liew, M. M. Glazov, A. V. Kavokin, G. Malpuech, and A. Bramati, Nat. Phys. **3**, 628 (2007).
[35] H. Ohadi, A. Dreismann, Y. G. Rubo, F. Pinsker, Y. del Valle-Inclan Redondo, S. I. Tsintzos, Z. Hatzopoulos, P. G. Savvidis, and J. J. Baumberg, Phys. Rev. X **5**, 031002 (2015).
[36] Y. N. Fernández, M. I. Vasilevskiy, C. Trallero-Giner, and A. Kavokin, Phys. Rev. B **87**, 195441 (2013).
[37] F. Tassone and Y. Yamamoto, Phys. Rev. B **59**, 10830 (1999).
[38] Within the envelope function approximation, the 2D susceptibility, $\chi_{2D} = p/(AE)$ (where p is the dipole moment and A is the area of the layer), is given by $\chi_{2D} = 2|\Psi_{ex}^{2D}(0)|^2\langle|\mathbf{e}\cdot\mathbf{d}_{ex}|^2\rangle(E_{ex} - \hbar\omega - i\hbar\gamma)^{-1}$. Here the factor of 2 stands for two spin orientations (or, equivalently, for two valleys), the square modulus of the exciton wave function can be taken within the simplest hydrogenlike model [47] as $2/(\pi a_{ex}^2)$, and the factor in angular brackets represents the transition dipole moment matrix element (squared) averaged over photon polarizations ($\mathbf{e}$). The optical conductivity is given by $\sigma_{2D} = -i\omega\chi_{2D}$.
[39] Y. V. Bludov, A. Ferreira, N. M. R. Peres, and M. Vasilevskiy, Int. J. Mod. Phys. B **27**, 1341001 (2013).
[40] J. Li, Y. L. Zhong, and D. Zhang, J. Phys.: Condens. Matter **27**, 315301 (2015).
[41] J. J. Hopfield, Phys. Rev. **112**, 1555 (1958).
[42] Usually the coupling constants are just fitted to reproduce the experimentally measured polariton dispersion [52].
[43] L. P. Pitaevskii, Sov. Phys. JETP **13**, 451 (1961).
[44] P. Meystre and M. Sargent III, *Elements of Quantum Optics* (Springer, Berlin, 2007).
[45] D. D. Solnyshkov, I. Shelykh, Y. Rubo, N. A. Gippius, and G. Malpuech, Phys. Rev. B **77**, 045314 (2008).
[46] A. Baas, J. P. Karr, H. Eleuch, and E. Giacobino, Phys. Rev. A **69**, 023809 (2004).
[47] C. Ciuti, V. Savona, C. Piermarocchi, A. Quattropani, and P. Schwendimann, Phys. Rev. B **58**, 7926 (1998).
[48] The numerical coefficient in this expression may depend on the model used [5].
[49] C. Trallero-Giner, T. C. H. Liew, and A. V. Kavokin, Phys. Rev. B **82**, 165421 (2010).
[50] L. Novotny and B. Hecht, *Principles of Nano-Optics* (Cambridge University Press, Cambridge, 2012).
[51] Y. V. Bludov and M. I. Vasilevskiy, J. Phys. Chem. C **116**, 13738 (2012).
[52] M. Slootsky, X. Liu, V. M. Menon, and S. R. Forrest, Phys. Rev. Lett. **112**, 076401 (2014).
[53] L. Ferrier, E. Wertz, R. Johne, D. D. Solnyshkov, P. Senellart, I. Sagnes, A. Lamaitre, G. Malpuech, and J. Bloch, Phys. Rev. Lett. **106**, 126401 (2011).
[54] G. Tosi, G. Christman, N. G. Berloff, P. Tsotsis, T. Gao, Z. Hazopolulos, P. G. Savvidis, and J. J. Baumberg, Nat. Phys. **8**, 190 (2012).
[55] G. P. Agrawal, *Nonlinear Fiber Optics* (Elsevier, Amsterdam, 2013).